EXPERIMENTAL ANALYSIS AND COMPUTATION OF THE ONSET AND DEVELOPMENT OF THE BOUNDARY LAYER TRANSITION

Daniel Arnal, Jean-Claude Juillen and Roger Michel
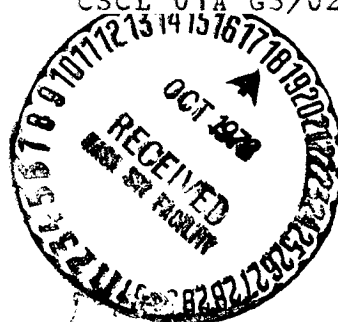
1. Report No. NASA TM-75325	2. Government Accession No.	3. Recipient's Catalog No.
4. Title and Subtitle EXPERIMENTAL ANALYSIS AND COMPUTATION OF THE ONSET AND DEVELOPMENT OF THE BOUNDARY LAYER TRANSITION		5. Report Date August 1978
		6. Performing Organization Code
7. Author(s) Daniel Arnal, Jean-Claude Juillen and Roger Michel		8. Performing Organization Report No.
		10. Work Unit No.
9. Performing Organization Name and Address .SCITRAN Box 5456 Santa Barbara, CA 93108		11. Contract or Grant No. NASw-2791
		13. Type of Report and Period Covered Translation
12. Sponsoring Agency Name and Address National Aeronautics and Space Administration Washington, D.C. 20546		14. Sponsoring Agency Code

15. Supplementary Notes

Translation of: "Analyse experimentale et calcul de l'apparition et du developpement de la transition de la couche limite," ONERA, Centre d'Etudes et de Recherches de Toulouse, Toulouse, France, (NATO, AGARD, Symposium on Laminar-Turbulent Transition, Copenhagen, Denmark, May 2-4, 1977), ONERA, TP No. 1977-54, 1977, 19 pp. (A77-44961)

16. Abstract

This study is concerned with the transition of an incompressible boundary layer, with zero pressure gradient and low free-stream turbulence. Mean velocity, turbulence and Reynolds shear stress profiles are presented. The development of the Tollmien-Schlichting waves is clearly shown until the turbulent spots appear. The intermittency phenomenon is studied by conditional sampling of the hotwire signal. The comparison with calculation results obtained by resolution of a set of transport equations shows a good agreement for the mean characteristics of the flow; discrepancies observed for the turbulent quantities evolution are due to the intermittency phenomenon.   (Author)

17. Key Words (Selected by Author(s))		18. Distribution Statement Unclassified - Unlimited	
19. Security Classif. (of this report) Unclassified	20. Security Classif. (of this page) Unclassified	21. No. of Pages 46	22.

EXPERIMENTAL ANALYSIS AND COMPUTATION OF THE ONSET AND DEVELOPMENT OF THE

BOUNDARY LAYER TRANSITION by Daniel Arnal, Jean-Claude Juillen and Roger Michel.

Office National d'Etudes et de Recherches Aérospatiales (ONERA) (National
Office of Aerospace Research and Studies)
Centre d'Etudes et de Recherches de Toulouse (CERT/DERAT) (Toulouse Study and
Research Center), 31055 Toulouse (France).

SUMMARY
This study is concerned with the transition of an incompressible boundary
layer, with zero pressure gradient and low free-stream turbulence. Mean
velocity,and turbulence and Reynolds shear stress profiles are presented.
We analyze the development of Tollmien-Schlichting waves until turbulent
spots appear. Conditional sampling of the hot-wire signal defines the
aspects of the intermittency phenomenon. Comparison with computation
results based on the resolution of a set of transport equations shows
good agreement for the average quantity levels; discrepancies attributed
to the intermittency phenomenon are noted in the evolution of turbulent
values.

NOTATIONS

x	abscissa measured on the axis from the stopping point
y	ordinate measured from the wall
t	time
$U(t)$, $V(t)$	instantaneous longitudinal and vertical velocities
U, V	average longitudinal and vertical velocities
u', v'	longitudinal and vertical fluctuations
$\overline{u'^2}$, $\overline{v'^2}$	quadratic mean of u' and v'
$-\overline{u'v'}$	Reynolds shear stress
ρ	air mass density
ν	kinematic viscosity

δ	physical thickness of the boundary layer
H	parameter defined as $H = \delta_1/\Theta$ called "shape parameter"
δ_1	displacement thickness $\delta_1 = \int_0^\delta (1-\dfrac{u}{u_e})dy$
Θ	momentum thickness $\qquad \Theta = \int_0^\delta \dfrac{u}{u_e}(1-\dfrac{u}{u_e})\,dy$
R_x, R_Θ	Reynolds numbers
f	frequency
Δf	analysis band (spectra)

Subscripts

e	outside the boundary layer
l	laminar
t	turbulent
p	pertaining to "spikes"

1 - INTRODUCTION

The purpose of the transition study undertaken by the CERT Aerothermodynamic Department is to determine the means of computation that eliminate to the maximum extent possible the empiricism inherent to the majority of currently-known methods. Therefore, from the start, the experimental results that are the subject of this paper were designed to check or define the hypotheses to use with such means of computation.

First, we wanted to consider the simplest experimental configuration, namely the case of an incompressible boundary layer without a longitudinal pressure gradient. The free-stream turbulence parameter is assumed to be the only one to affect the triggering of the transition; we are therefore in the presence of a "natural transition" where there are none of the artificial devices frequently used to study this phenomenon (vibrating tape, controlled three-dimensionality, and electrical discharges creating turbulent spots).

2

First, we attempted to obtain an overall description of the phenomenon from the laminar condition to the turbulent regime by means of detailed measurements of mean velocity, and turbulence and Reynolds shear-stress profiles. It then appeared that these values obtained with averages over a theoretically infinite period of time were insufficient to really understand the mechanisms for creating and developing the turbulence. A second study phase based on the conditional analysis of the instantaneous speeds $U(t)$ and $V(t)$ was thus undertaken. It made it possible to thoroughly study certain aspects of the transition process, particularly the characteristic intermittency of a transitional flow, through a separate study of the two types of flow (laminar and turbulent) which follow each other at a given point as a function of time. The comparison of experimental results with numerical results obtained by resolving a model with two transport equations shows that this intermittency phenomenon does not appear in modelling and keeps computations from accurately reproducing the evolution of turbulent values.

2 - EXPERIMENTAL MOCK-UP - MEANS OF MEASUREMENT

2.1. - Facility and Test Conditions

The experimental study was performed in a subsonic wind tunnel shown in a photograph and schematic in Figure 1. The transition is studied over a cylindrical body with a 6 cm diameter with an ogive-shaped tip and placed along the axis of a cylindrical stream with a 20cm diameter. The overall length of the center body is 1.2 meter.

With the configuration studied, the overall velocity U_e is constant and equal to 33 m/sec with a turbulence rate $\sqrt{\overline{u'^2}}/U_e$ of about 0.25%.

2.2. - Measuring Equipment

The basic wind measuring system consists of hot-wire anemometers at constant temperature (straight wire and crossed wires), rectifiers and bandpass filters. A slow acquisition system (10 points per second) makes it possible to obtain the mean velocity, and turbulence and Reynolds shear-stress profiles as well as the characteristic parameters of the boundary layer.
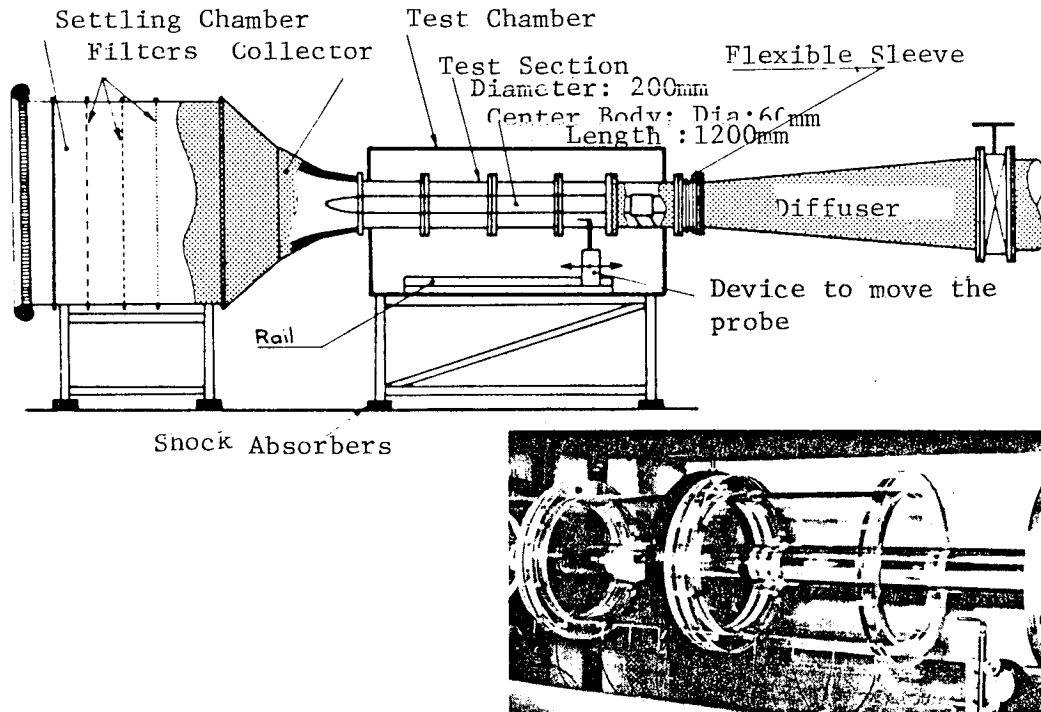
Figure 1 : Experimental Set-Up.

A significant portion of this study is composed of the conditional sampling of the instantaneous velocities U(t) and V(t). To that end, the signals provided by the hot wires are first recorded in an analog form; we then digitize the data by means of an analog-digital converter. The magnetic tape obtained in this manner is processed in a computer. At every test point digitization takes place over 6 seconds at the rate of 10,000 points per second. Therefore, we perform an analysis with 60,000 points.

3 - OVERALL STUDY OF THE TRANSITION

Here, the expression "overall study" refers to the examination of the raw data provided by the wind-measuring systems by making averages over

4

sufficiently long periods of time. The quantities studied are the mean velocity U, the turbulence energies $\overline{u'^2}$ and $\overline{v'^2}$, and Reynolds shear-stress $-\overline{u'v'}$.

3.1. - Mean Velocity Profiles and Integral Values

A systematic exploration of the boundary layer was undertaken from the abscissa x=0.66m to the abscissa x=1.19. In Figure 2, we plotted the velocity profiles obtained.
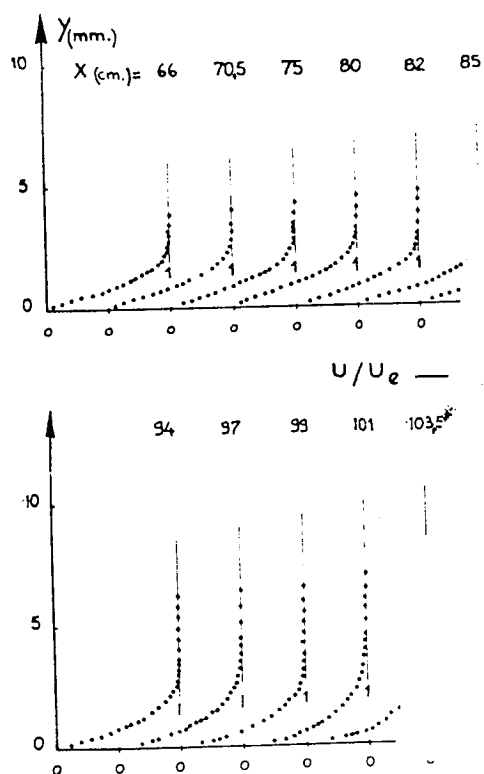
Figure 2 - Average Velocity Profiles.

Figure 3 shows the evolution of the characteristic parameters of the boundary layer: the shape parameter H and the Reynolds Number created with the momentum thickness Θ.
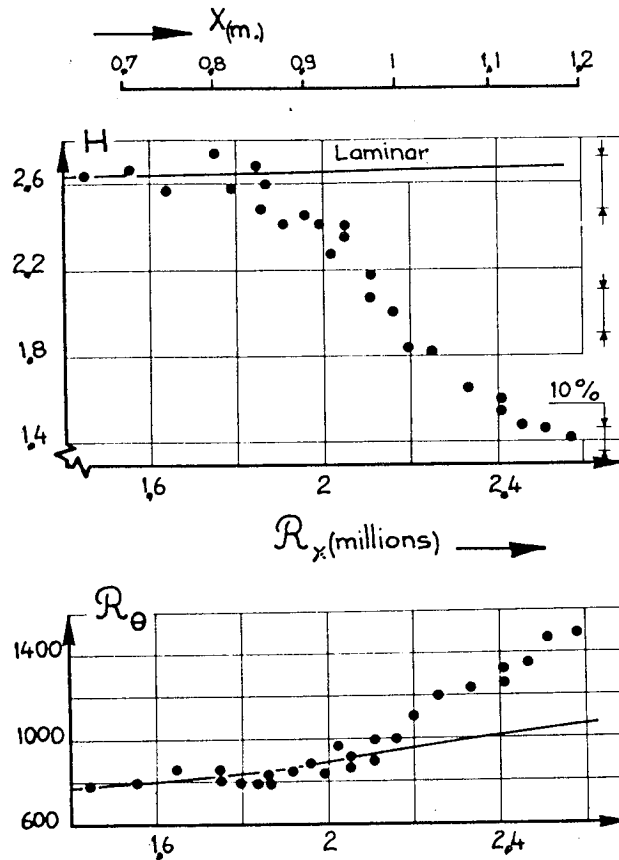
Figure 3 - Evolution of the Integral Values of the Boundary Layer.

Up to an abscissa of about 0.80 meters, the shape parameter remains near 2.6 (Blasius profile); it then decreases to approach a value of about 1.4. The curve shown as a continuous line is the result of laminar computations performed from the stopping point. The theoretical value of H, somewhat greater than the one in a Blasius profile, is explained by a very small longitudinal pressure gradient.

3.2. - Profiles of Turbulent Values

The profiles of $\overline{u'^2}$, $\overline{v'^2}$ and $-\overline{u'v'}$ are plotted on figures 4, 5 and 6 where
we also show several recordings of the instantaneous longitudinal fluctuation
u'(t). The turbulent drag profiles shown with white circles come from a
slow measurement system; those shown with dark circles come from digitization
results. We can note that the evolution of the $\overline{u'^2}$ profiles as a function
of the abscissa is similar to the one provided by the experiments conducted
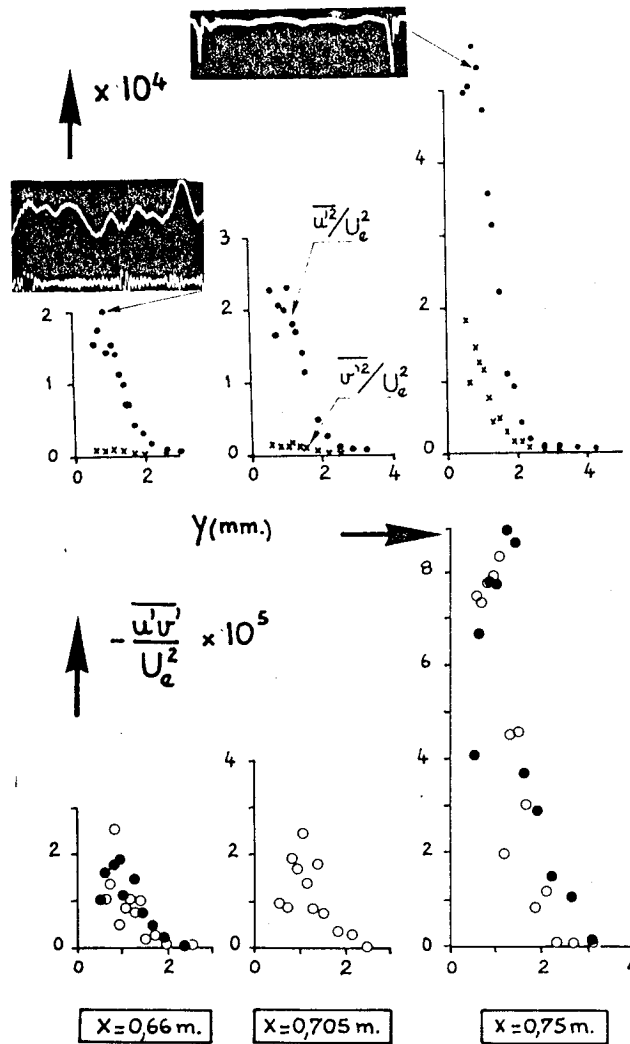by Schubauer and Klebanoff (1).

Figure 4 - Turbulence and Reynolds Shear-Stress Profiles(1).

3.2.1. - Laminar Regime

The title "laminar regime" defines the study area that extends to the inevitably inaccurate abscissa where the turbulence first appears.

Within this area (Figure 4) we first notice no significant changes in the profiles between x=0.66m and x=0.705m; vertical fluctuation energy remains far less than the energy in the longitudinal fluctuation and turbulent drag is low: the maximum value of the $-\overline{u'v'}/U_e^2$ ratio does not exceed 3×10^{-5} while the local drag coefficient is in the order of 5×10^{-4}. It is only when x=0.75m that we observe a considerable increase in the turbulence and Reynolds shear-stress levels; the examination of the instantaneous signals can help to understand this rapid evolution.

At x=0.66m, the instantaneous velocity is made up of a low-amplitude steady high-frequency oscillation (about 600 Hz) and of a carrier wave with an irregular shape of lower frequency and higher amplitude. The filtered signal eliminates frequencies lower than 150 Hz. It reveals the fact that the high-frequency oscillation has a sinusoidal shape showing the effect of modulation. The sinusoidal wave corresponds to the Tollmien-Schlichting waves, the existence of which in a natural transition was actually later revealed by Schubauer and Skramstad (2). These waves will be more accurately studied in Chapter 5.

At x=0.75m (note that here the signal amplification is 10 times less that the amplification at x=0.66m), the signal u'(t) still shows the presence of Tollmien-Schlichting waves and of the low-frequency carrier. In addition, it reveals the existence of negative fluctation "spikes" that are few in number but that have considerable amplitude. These spikes, studied by Schubauer, Tidstrom, Sargent (3) and by Kovasznay, Komoda, Vasudeva (4) have significant energy but are too few in number to appreciably modify the mean velocity profile.

3.2.2. - The Actual Transition

In the first part of the transition (Figure 5), the maximum value of $\overline{u'^2}$
increases rapidly and comes closer to the wall. At x=0.94m, the recording
of the instantaneous longitudinal velocity shows that the hot wire is
successively immersed into turbulent areas ("spots") characterized by high-
frequency fluctuations and within laminar regions that are more or less
rectilinear. This is the intermittency phenomenon that we will describe
in detail in Chapter 5. The recording made at x=0.8m shows turbulent spots
as well as fluctuation spikes similar to those already described. The
maximum value of turbulent drag increases rapidly; it is moreover striking
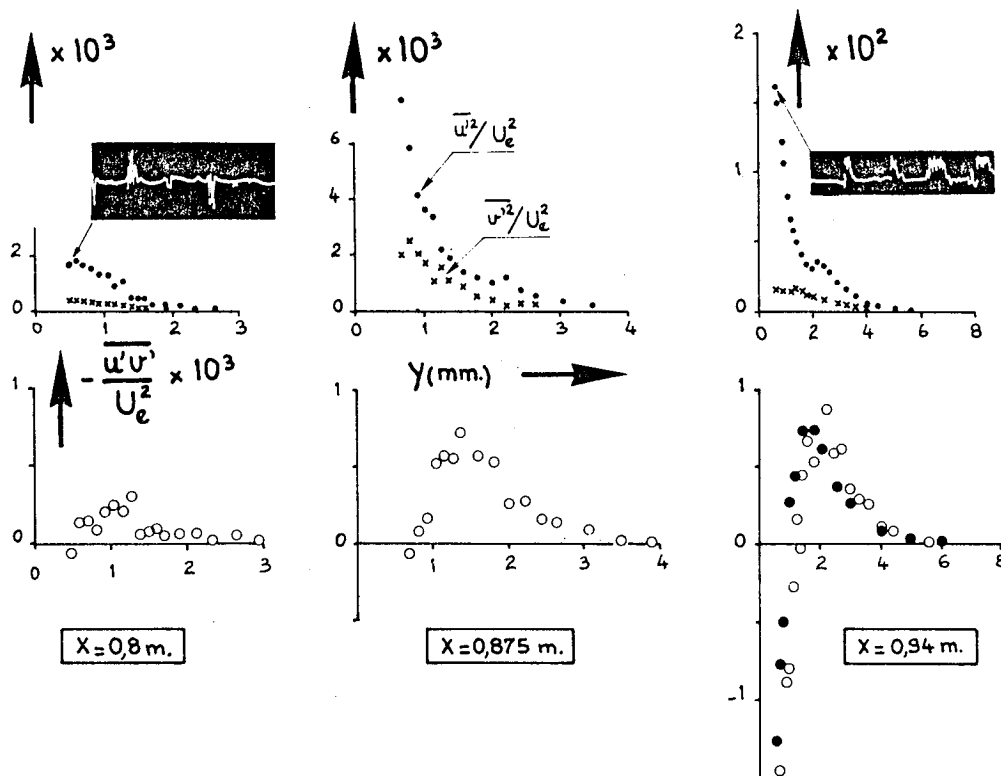to note that near the wall, the drag $-\overline{u'v'}$ takes negative values.

Figure 5 - Turbulence and Reynolds Shear-Stress Profiles (2).

As the $\overline{u'^2}$ maximum close to the wall develops, a second maximum appears (x=0.94m); it changes very little in the second part of the transition Figure 6), maintaining a nearly-constant value ($\sqrt{\overline{u'^2}}/U_e \approx 8\%$). Beyond the abscissa x=1.01m, the value of the maximum near the wall decreases. We note that this maximum has not completely disappeared at the last station, where the turbulent flow has not yet been entirely established.

Moreover, we will note that the shape of the profiles of $\overline{v'^2}$ changes very little within the transition region: they show a monotonic decrease from the wall to the outside of the boundary layer; as a result, the $\overline{u'^2}/\overline{v'^2}$ ratio has a shape reminiscent of the $\overline{u'^2}$ profiles with, in particular, the existence of two maxima starting with x=0.94m.

The negative portion of the $-\overline{u'v'}$ profiles disappears little by little when we approach the end of the transition. The last probe station shows a profile that is not very different from an established turbulent profile.
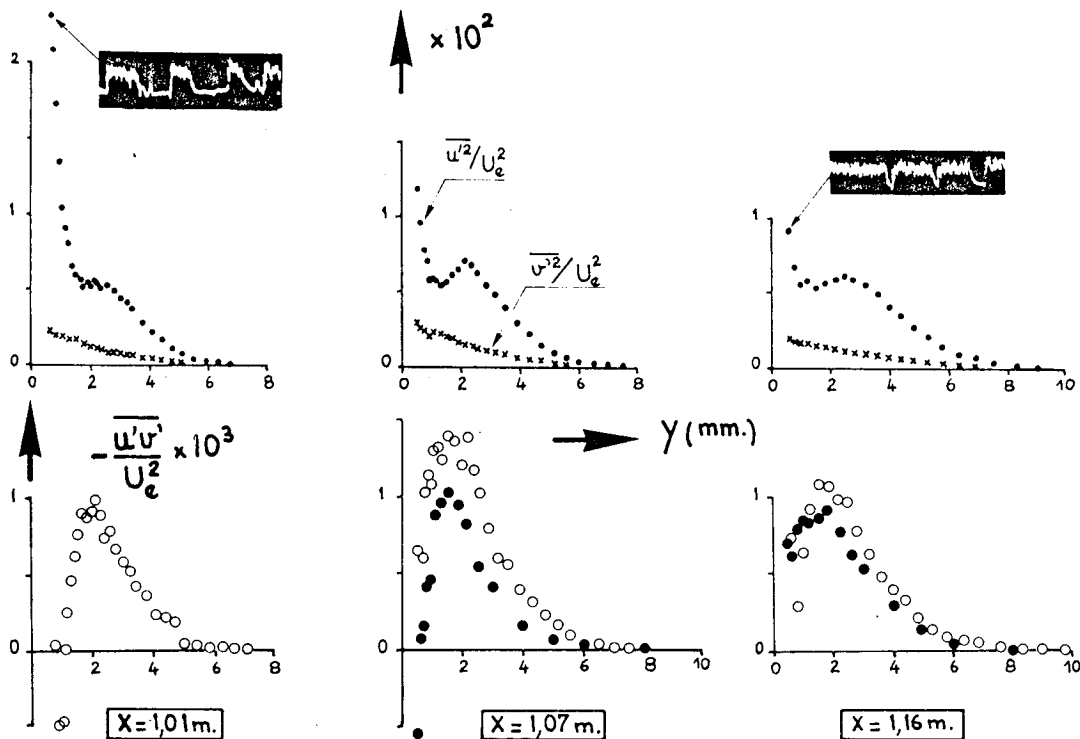

Figure 6 - Turbulence and Reynolds Shear-Stress Profiles (3).

10

4 - GENERALITIES ON CONDITIONAL SAMPLING

The overall study that we have just presented shows the complexity of the
transition phenomenon, the sporadic appearance of fluctuation spikes, and
the intermittent nature of the actual transition regime. All of this
information does not appear in the rough profiles of mean velocity,
and turbulence and Reynolds shear-stress. Therefore, it is necessary to
complete the study of these overall results by means of a conditional
sampling of the instantaneous velocities U(t) and V(t) in order to separately
characterize the various types of flow that we can encounter at a given point
of measurement.

The definitions and notations given below will apply to the specific case
of an intermittent laminar-turbulent flow. Of course, we will be able to
stretch them and to adapt them to any other flow characterized by the
succession and alternation of several states (for example, the alternation
of the fluctuation points and of the laminar areas).

4.1. - Intermittency Function
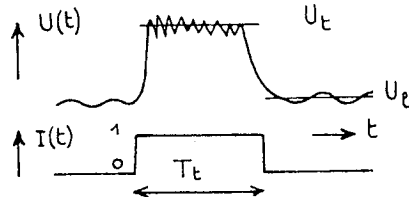
Let us consider the instantaneous velocity U(t) within an area of intermittency
where turbulent spots and laminar areas follow each other. In the first place,
we seek   to discriminate, without any ambiguity, these two types of
flow: we build a function called "all or nothing", I(t), which is named the
intermittency function and which has a zero value in laminar areas and a 1 value
in turbulent areas. The construction of the function I(t) starting from the
distribution function of a detection signal D(t) is given in (5) and (6).

With I(t) determined, comparing it with the signal U(t) makes it possible
to compute overall averages against time and overall averages with a fixed t/T.

4.2. - Overall Averages Against Time

The average I(t) performed over the entire sampling time is the intermittency
factor γ:

$$\gamma = \lim_{t_0 \to \infty} \frac{1}{t_0} \int_{t_1}^{t_1+t_0} I(t) \, dt$$

In fact, γ represents the fraction of the total time during which the
flow is turbulent.

We define the average turbulent and laminar speeds as:

$$U_t = \frac{\overline{I(t) \quad U(t)}}{\gamma} \qquad \text{and} \qquad U_\ell = \frac{\overline{(1-I(t)) \quad U(t)}}{1 - \gamma}$$

We can still define "laminar fluctuations" u_ℓ' and "turbulent fluctuations"
u_t' such that:

$$u'_t = U(t) - U_t \quad \text{if } I(t) = 1$$

$$u'_t = 0 \quad \text{if } I(t) = 0$$

$$u'_\ell = U(t) - U \quad \text{if } I(t) = 0$$

$$\text{and} \quad u'_\ell = 0 \quad \text{if } I(t) = 1$$

We then check that we have:

$$\overline{u'^2} = \gamma \, \overline{u'^2_t} + (1-\gamma) \, \overline{u'^2_\ell} + \gamma(1-\gamma)(U_t - U_\ell)^2$$

If the function I(t) is the same for U(t) and V(t), we also have:

$$\overline{v'^2} = \gamma \, \overline{v'^2_t} + (1-\gamma) \, \overline{v'^2_\ell} + \gamma(1-\gamma)(V_t - V_\ell)^2$$

$$\overline{u'v'} = \gamma \, \overline{u'_t v'_t} + (1-\gamma) \, \overline{u'_\ell v'_\ell} + \gamma(1-\gamma)(U_t - U_\ell)(V_t - V_\ell)$$

Therefore, we note that the approximate values considered in chapter 3 ($\overline{u'^2}$, $\overline{v'^2}$ and $\overline{u'v'}$) are in fact the sum of a turbulent component, a laminar component, and a component coming from the difference in the laminar and turbulent average velocities. We will call this sum, the "slot component".

4.3. - Overall Averages with a Given t/T_t

If T_t represents the duration of a turbulent spot and if t is the time measured from the beginning of the spot, we compute the average of U(t) over a large number of spots for a given t/T_t value. Such an average will be labelled $\langle U_t \rangle$.

5 - DETAILED STUDY OF THE TRANSITION

This chapter covers in depth the fundamental aspects of the transition process. To that end, a certain number of abscissas characterized by typical phenomena have been selected and analyzed in a detailed manner. Within the area where laminar flow takes place without any "peaks", the abscissa x=0.66m is studied, primarily because of the presence of Tollmien-Schlichting waves which represent a manifestation of instability in the laminar boundary layer. The abscissa x=0.75m indicates the end of the laminar regime. There, we will examine the effect of the passage of spikes and the appearance of the first turbulent spots. We will finally be interested in the intermittent transitional regime at the level of stations x=0.87m, x=0.94m, and x=1.07m. The conditional sampling of the instantaneous velocity represents the main tool for this study.

5.1. - Laminar Regime Without Spikes (x=0.66m)

Let us recall that at this abscissa, the fluctuation u' is composed of Tollmien-Schlichting waves and a low-frequency carrier.

5.1.1. - Coarse Signal

Figure 7 shows the evolution along y of the coarse instantaneous signal U(t).

We compare the simultaneous recordings of a reference signal near the wall (y_0=0.4mm) and of a signal at a variable y altitude. Since the vertical scale is not the same for all recordings, we have indicated the relative amplification of the signal U(t,y) relative to signal U(t,y_0). It is clear that the amplitude of the Tollmien-Schlichting is low relative to that of the carrier.
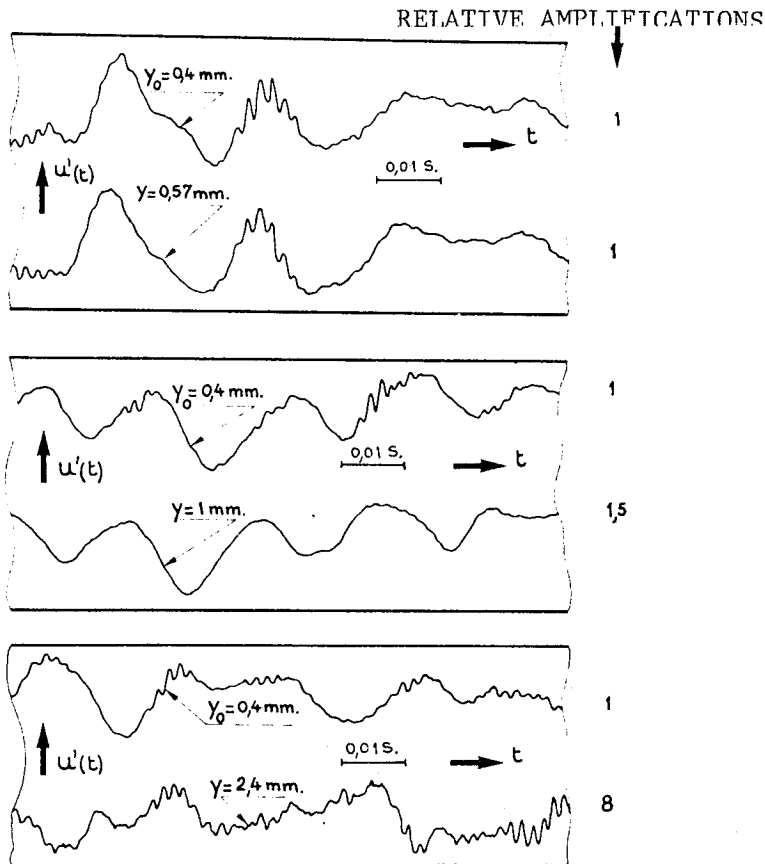

Figure 7 - Recordings of u' (x=0.66m).

Frequency analysis of the signal U(t) shown in Figure 8 illustrates quantitatively this last observation. In the upper section of the figure, we show three spectra obtained at different altitudes within the boundary layer. Most of the energy is concentrated in low frequencies below 200 Hz. At y=0.52mm, we observe-at about 600 Hz-a deformation of the spectrum corresponding to the Tollmien-Schlichting waves, a deformation that no

14

longer appears at y=1.52mm and at y=4mm. (The spectrum associated with this last altitude in fact represents the spectrum of the free-stream turbulence). The lower portion of Figure 8 shows the evolution of the amplitudes for different frequencies: the preponderance of low-frequency fluctuations still appears. We have noted that these fluctuations presented probability densities very close to the normal rule and that their leveling factor did not move far from the value of 3, from the wall to the free-stream flow. We can assume that low frequency fluctuations are associated with the existence of a relatively significant external turbulence and that they therefore represent the response to a forced oscillation. The Tollmien-Schlichting waves described in the following paragraph result from an entirely different process since they are oscillations within the laminar boundary layer.
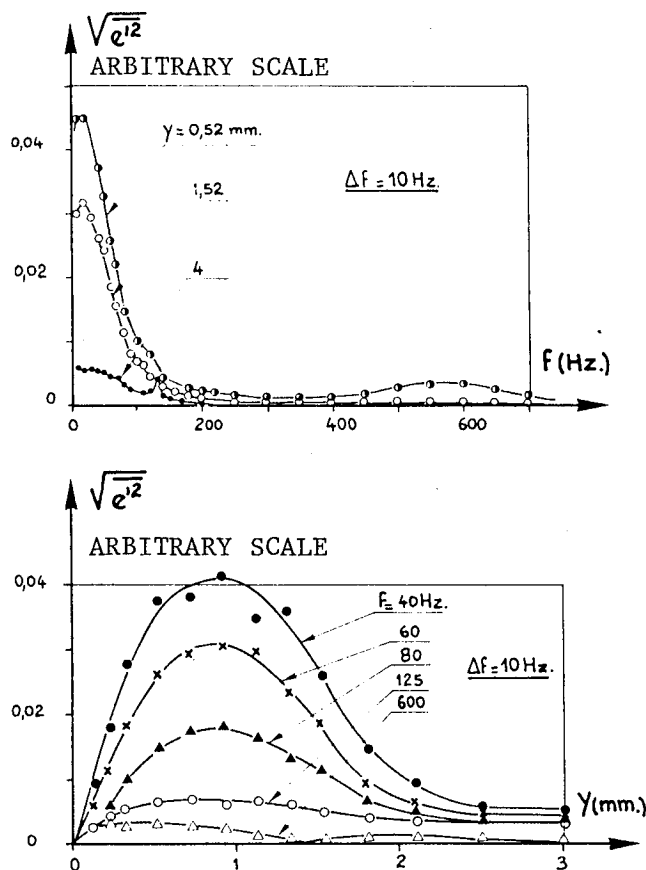

Figure 8 - Spectral Study in a Laminar Regime.

5.1.2. - Tollmien-Schlichting Waves

The theory of laminar instability which describes the behavior of the
Tollmien-Schlichting waves has been the subject of numerous works (see
for example, Schlichting (7), Jordinson (8), Gaster (9), and Fasel (10).
Its experimental verification has been performed by different authors,
either in the case of waves artificially created with a vibrating tape
(Schubauer-Skramstad (2), Ross-Barnes-Burns-Ross (11)) or more seldom
in the case of natural instabilities (Burnel-Gougat (12)). The oscillations
recorded in these experiments belong to this last category.

In Figure 9, we show the shape of the signal U(t) after filtering the
low frequencies. As for the coarse signal, a probe placed at y_0=0.4mm
remains fixed; another probe is placed at various altitudes and we
simultaneously record the signals provided by the two probes. Here, the
vertical scale is identical for every pair of recordings. The waves
recorded at y=0.57mm are in phase with the reference waves while those
at y=2.4mm are of opposite phase. At y=1.5mm, the amplitude of the
oscillations proves to be negligible. We have been able to prove that
it is at this altitude that the phase shift mentioned before takes place.
These observations are in agreement with the theory of laminar instability.
Moreover, we can note that the effect of amplitude modulation simultaneously
affects the entire thickness of the boundary layer (see in particular the
signals recorded at y_0 and y=2.4mm). However, this modulation exceeds
the framework of the theory of laminar instability in which the amplitude
of the waves remains constant in time at a given point (Burnel-Gougat (12)).

The profiles of average amplitudes of the oscillations u' and v' of the
600Hz frequency are plotted in Figure 10. We can properly check that the
amplitude of u' is cancelled at y≃1.5mm; at the same altitude, the
amplitude of v' reaches its maximum value. The amplitude of u' is then
increasing, reaches a second maximum at y≃2.4mm and finally decreases as
does the amplitude of v' to become zero in the free-stream flow. The theory of
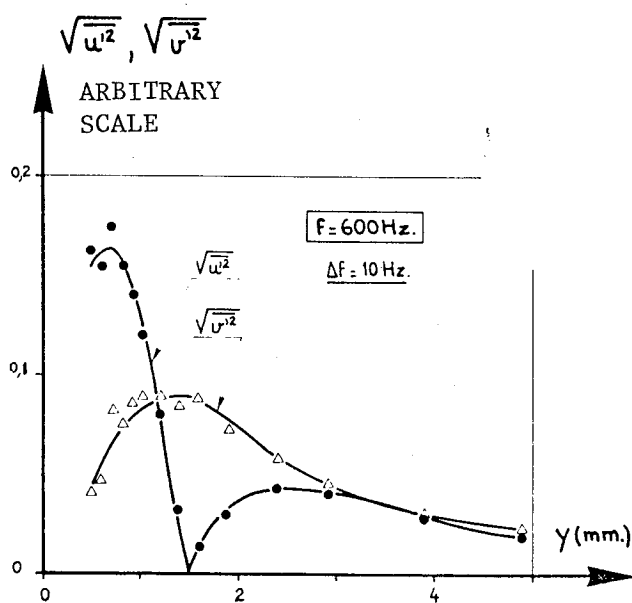
16
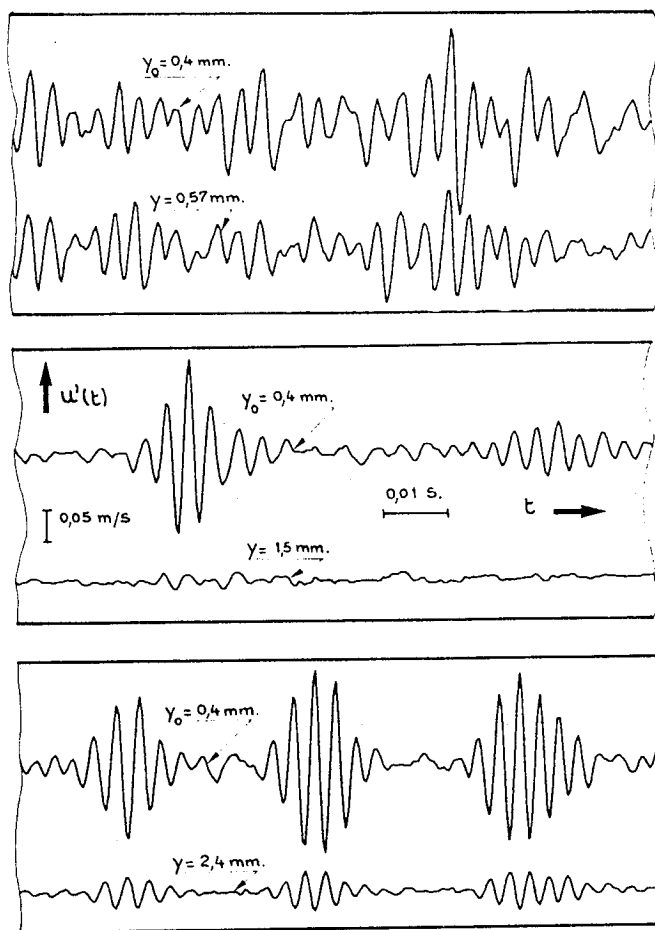
Figure 9 – Tollmien-Schlichting Waves – Recordings.

Figure 10 – Tollmien-Schlichting $-\sqrt{\overline{u'^2}}$ and $\sqrt{\overline{v'^2}}$ profiles.

laminar instability predicts this evolution. Through the mathematical
form of the flow function from which the u' and v' fluctuations are
derived, the maximum amplitude of v' takes place when the amplitude of
u' is zero.

5.2. - End of the Laminar Regime (x=075m)

In the sequence of events leading from the laminar regime to the appearance
of the turbulent spots, we have seen (Paragraph 5.1) that the first stage
was correctly described by the theory of laminar instability. By following
the classification proposed by Tani (13), the second phase of the transition
process is characterized by the appearance of a pronounced three-dimensionality
of the Tollmien-Schlichting waves which then behaves differently
from the linearized two-dimensional theory. In the third phase, a shear
layer is formed which is seen, over the shape of the signal U(t), through
the presence of negative fluctuation spikes. It is this   phase that is
most particularly studied in this paragraph. We will also cover the fourth
and last phase: the onset of turbulent spots.

5.2.1. - Qualitative Study

A few examples of recordings of the signal u'(t) are presented in Figure 11.
As before, these recordings are simultaneous, taken two at a time, with a
probe remaining fixed at y_0=0.4mm and the other being placed at various
altitudes.

The two signals at the top of the figure have the shape that is the most
frequently encountered at x=0.75m: negative fluctuation "spikes" of
considerable amplitude affect the entire thickness of the boundary layer.
In fact, at the abscissa considered, these spikes go in pairs: this state
has been called "double-spike stage" by by Kovasznay-Komoda and Vasudeva (4)
as opposed to the "single-spike stage" that precedes it and that is
characterized by isolated negative spikes.

18
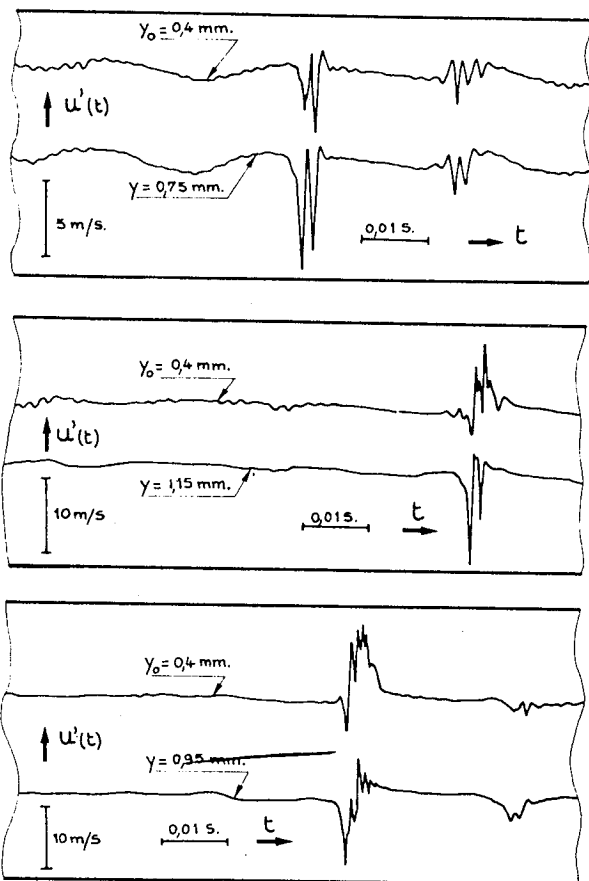
Figure 11 - Recordings of u' (x=0.75m).

The other four recordings correspond to a later stage in the transition process since they show the appearance of turbulent spots. It is important to note that this type of signal is met more frequently than the previous ones at the abscissa under study.

Let us first consider the two signals recorded at y_0 and at $y=1.15mm$. At this last altitude, we encounter the same shape as before: two consecutive negative spikes. But, at y_0, although we have a first negative spike, there is a series of positive spikes immediately thereafter. The two recordings presented at the bottom of Figure 11 indicate, at altitude y_0, an overall

rise in instantaneous velocity for about 0.004 second accompanied by
fluctuations with a frequency that can be estimated at 1200Hz. Here,
we recognize the classical shape of turbulent spots near the wall (see
Figures 5 and 6). At y=0.95mm, the corresponding instantaneous signal
displays the two negative spikes that also precede high-frequency
fluctuations. However, the shape of the signal does not reflect the
appearance of a turbulent spot as well as near the wall.

5.2.2. - Qualitative Study
A preliminary quantitative analysis of the signals U(t), a few examples
of which have been given, is shown in Figure 12. Having observed that
within the periods of time that the flow maintains laminar characteristics
the fluctuation u' does not exceed $\pm$2m/sec, we have plotted as a function
of y the probability $\mathcal{P}$ of having a fluctuation less than -5m/sec and
-10m/sec. The evolution of these curves along y makes it possible to
determine the altitude where the negative spikes have, on the average,
the highest amplitude. We have also plotted on this figure the probability
$\mathcal{P}$ of having a fluctuation u' greater than 5m/sec and 10m/sec. Thus, it
appears that the existence of significant positive fluctuations is localized
to the area near the wall. (The term "positive fluctuations" includes, of
course, the turbulent spots being formed like the one recorded at y_0 for
the simultaneous signals at the bottom of Figure 11).

For now, we will use the subscript p for the quantities pertaining to
fluctuation spikes, either positive or negative. The intermittency pseudo-
factor γ_p, the ratio of the duration time of these spikes to the total time,
is in the order of 3×10^{-2} at the abscissa under consideration.

The breakdowns of turbulent energy $\overline{u'^2}$ and of Reynolds shear-stress $-\overline{u'v'}$
into their three components (laminar, contribution of the spikes, "slot"
term) are shown in Figure 13. The detection function chosen here is very
simply the absolute value of u'. The profiles corresponding to the laminar
terms are completely comparable to the profiles of $\overline{u'^2}$ and $-\overline{u'v'}$ recorded
in a non-disturbed laminar regime at x=0.66m and x=0.705m (Figure 4).
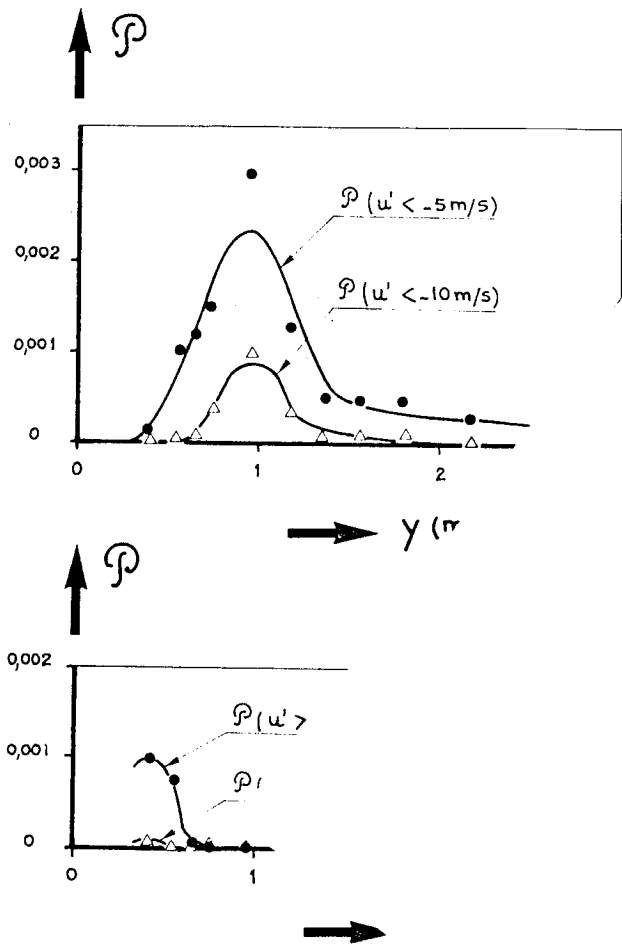
20

Figure 12 : Probability Density of the Negative and Positive Spikes.

We checked to see if this also applied to $\overline{v'^2}$. The passage of spikes therefore contributes considerably to the creation of turbulent energy and of turbulent drag. Although representing only three per cent of the sampling time, these spikes provide 50 per cent of the overall $\overline{u'^2}$ and $\overline{u'v'}$.

Negative u' Spikes: We are now interested only in the single negative fluctuation spikes, that is to say the state called "double-spike stage" by Kovasznay-Komoda, Vasudeva(4). Quantities associated with these negative spikes will again be indicated with the subscript p. At the abscissa under

study we detect 16 of them per second and an average duration of 3.5msec.
(more precisely, we detect 8 pairs of negative spikes per second). u' is
the detection function used with a negative threshold.

The evolution of the quantities $V_p - V_\ell$ and $U_p - U_\ell$ as a function of
altitude is given in Figure 14. We will first note that $U_p - U_\ell$ is
negative while $V_p - V_\ell$ is positive. The $U_p - U_\ell$ and $V_p - V_\ell$ curves
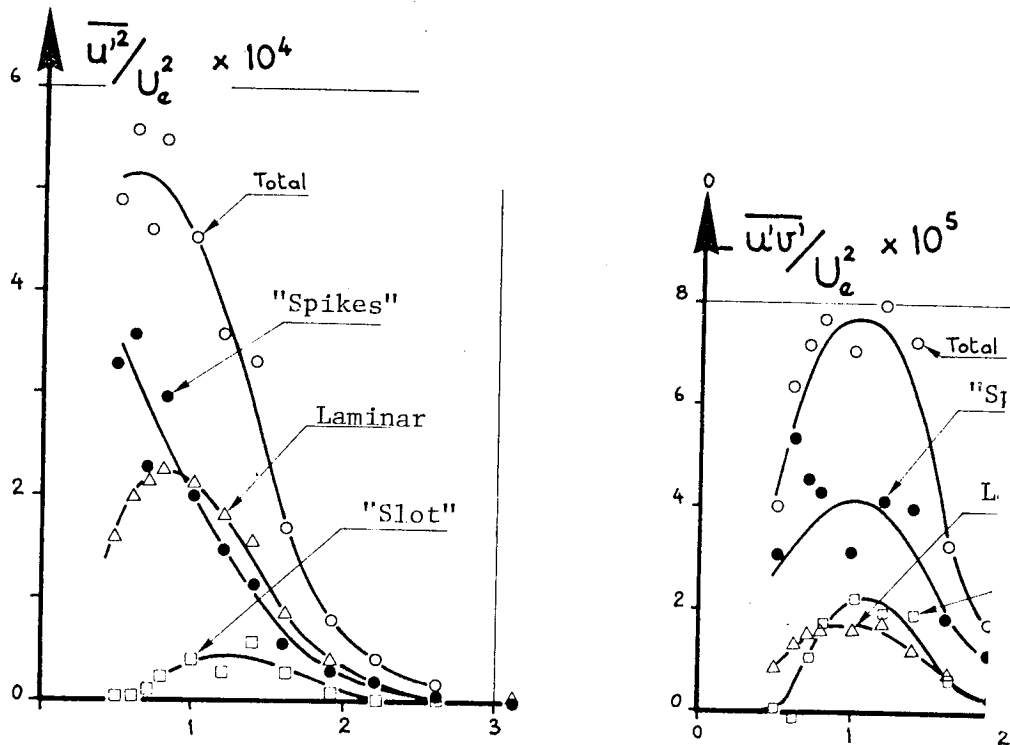respectively reach a minimum and a maximum at y≃1mm.

Figure 13 - Breakdown of $\overline{u'^2}$ and $\overline{u'v'}$ (x=0.75m)
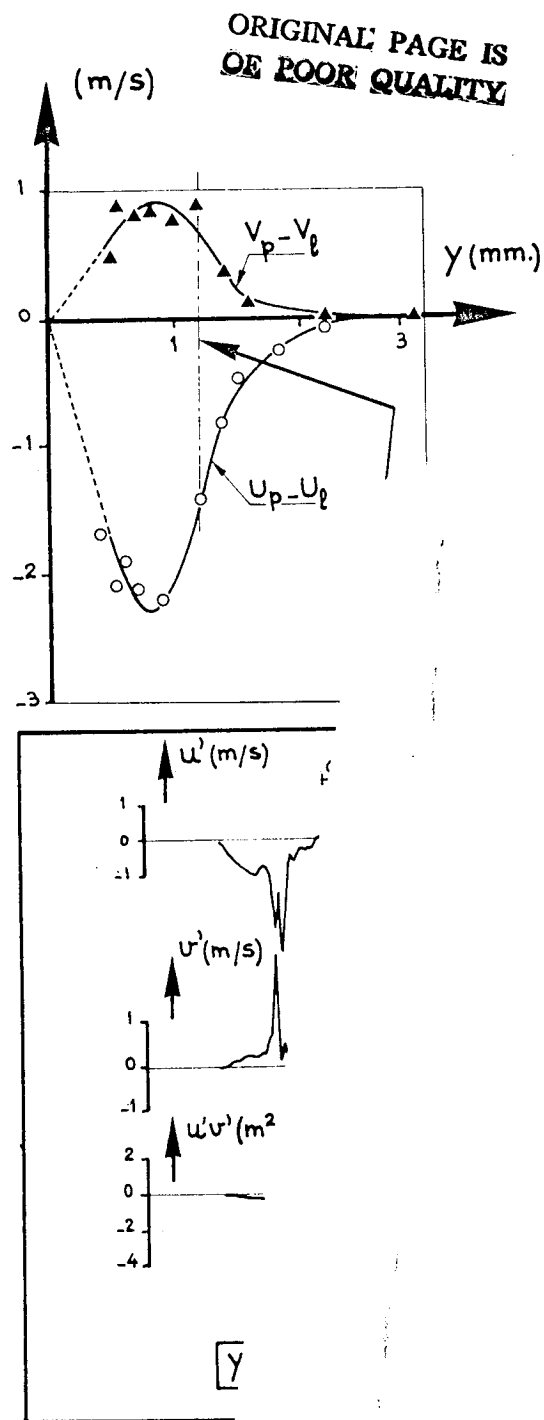
22

Figure 14 – $U_p - U_\ell$ and $V_p - V_\ell$ Profiles (x = 0.75m).

Of course, this is the altitude corresponding to the largest probabilities of observing significant negative fluctuations. An example of a simultaneous recording of the u' and v' fluctuations, as well as their product u'v', is also shown in Figure 14. We will particularly note the considerable amplitude of the instantaneous Reynolds shear-stress. The $-u'v'/U_e^2$ ratio reaches a maximum value of 5.8×10^{-3} during the passage of the first spike.

The overall averages at a given t/T_p define the effect of the negative u'
spikes on the instantaneous velocity profile. Indeed, T_p proved itself
to be practically independent of the spike amplitude and of boundary layer
altitude. The value found is 1.6ms which corresponds approximately to a
period of the Tollmien-Schlichting waves. By working with the signals
simultaneously delivered by the two hot wires, one at a constant y_0 (0.4 mm)
and the other at a variable y distance, we can stop in time the overall
averages obtained at y_0 and y. Examples of $<U_p>(t)$ curves for different
values of the y parameter are shown on the left side of Figure 15. Here,
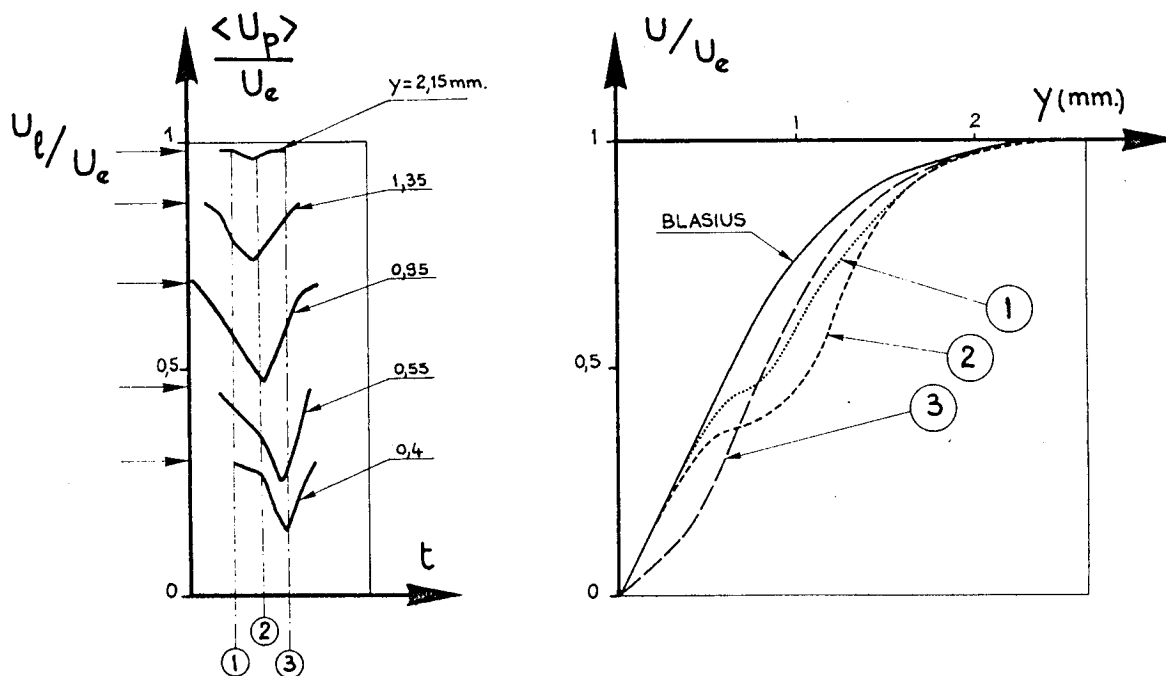

Figure 15 - Study of the Negative u' Spikes (x=0.75m)

only the negative spikes providing fluctuations with a minimum u' value
less than -4m/sec at y_0 have been considered. It appears that the spikes
do not reach their maximum amplitude at the same time; near the wall, the
passage of the spikes is later than at higher altitudes. Another presentation

24

consists of plotting the instantaneous velocity profiles by considering
the values of $<U_p>$ at different times which are indicated on Figure 15
with ①, ② , and ③ . The corresponding instantaneous profiles are
shown on the right side of Figure 15. As compared with the Blasius profile,
a deformation is first seen when 0.5mm$<y<$2mm (① Profile). This deformation
is accentuated (② Profile) and provides an increasingly noticeable
inflection point at an altitude of about 0.7mm. The last profile shows
that the proximity of the wall is then affected while the deformation of
the ① and ② Profiles decreases beyond y=0.7mm.

These results are in qualititative agreement with the experiments conducted
by Kovasznay et al (4) and Klebanoff et al (3), authors who studied this
phase of the transition process by exciting the boundary layer with a
vibrating tape and by imposing the three-dimensionality of the flow by
using adhesive tape strips attached to the wall. The negative u' spikes
(and the positive v' spikes are the indication of the passage of a vortex
having the shape of horseshoe in the x-z plane ("horseshoe vortex") and
resulting from the three-dimensional deformation of the Tollmien-Schlichting
waves. Visualizations in air by Knapp-Roach-Mueller (14) and in water by
Hama-Long-Hegarty (15), for example, have clearly shown this deformation.
In the x-y plane, the horseshoe vortex is inclined relative to the wall,
its "head" is located at $y/\delta \approx 0.5$ (Kovasznay et al (4)). This description
is compatible with the observations that we have just performed in the case
of a natural transition. It is in this manner that the inclination of the
vortex relative to the wall can explain the fact that the instantaneous
velocity profile is first deformed near the middle of the boundary layer
(passage of the "head") before the deformation reaches areas that are
increasingly closer to the wall. Nevertheless, let us note that in this
case, the u' and v' spikes appear in a random manner while the control of
three-dimensionality in the experiments described in references (3) and (4)
require well-defined longitudinal and transversal wavelengths.

Positive u' Spikes - Appearance of the Turbulent "Spots"

We have seen that in the U(t) recordings made near the wall, positive
spikes (or a turbulent spot) sometimes appear immediately after the first
negative spike. As we have just seen, the latter has a destabilizing
effect by creating an inflection point on the instantaneous velocity
profile.

An attempt to determined the most likely altitude for the appearance of
these positive spikes or of these spots was made in the following manner:
at the altitude $y_0 = 0.4$mm, we detect the passage of the positive spikes
or of the spots (detection function u' with a positive threshold) and,
from the simultaneous recordings at other altitudes, we compute
the average longitudinal velocity at a given y during these times of
passage. In this manner, we obtain a $U_p(y)$ profile depicting the average
profile inside the boundary layer when a more-or-less shaped spot passes
y_0. This profile is shown in Figure 16 where we compare it with the
classical average velocity profile. For y>about 1mm, the passage of a
spot at y_0 does not manifest itself as any appreciable change in the
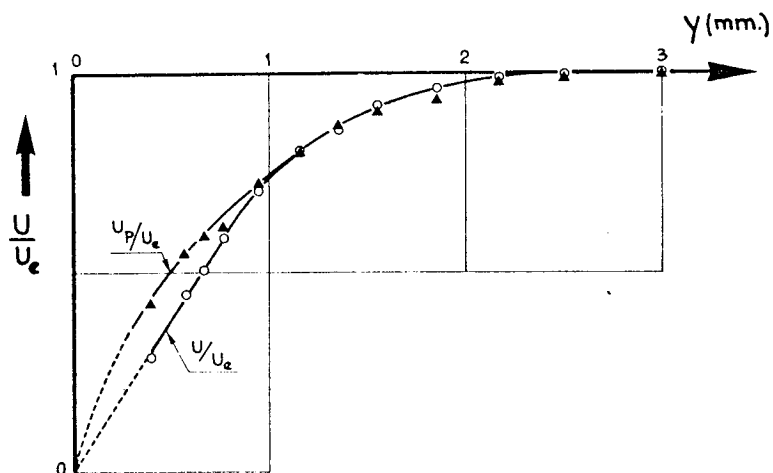average velocity profile.

Figure 16 - U_p Profile at the Onset of the Spots.

We can conclude from this that it is below the altitude where the negative spikes have the greatest amplitude that the spots appear by giving rise to overspeeds relative to the average profile.

5.3. - Study of the Intermittency Phenomenon

In the case of a natural transition, the generation of the turbulent spots is a random process as was suggested by Emmons (16). Nevertheless, let us note that it is possible to control the intermittency, for example in the case of a pulsed free-stream flow (Cousteix-Houdeville- Desopper (17)).

The study of the development of the turbulent spots has interested several authors, particularly Schubauer-Klebanoff (1), Elder (18), Wygnanski-Sokolov-Friedman (19) who have reapplied the experimental technique developed by Mitchner (20), namely the creation of artificial spots using electrical discharges. In the case of the present experiments, the intermittency phenomenon characterized by the alternation of spots and laminar areas was studied through conditional sampling of the U(t) and V(t) signals at three abscissas respectively located at the beginning, middle and end of the transition area. Below, we will recall the H shape parameter for these three stations:

X(m)	0.87	0.94	1.07
H	2.55	2.09	1.64

5.3.1. - Qualitative Study

Figure 17 shows a few typical sample recordings of the U(t) signal near the wall, at the three previously mentioned stations. We observe that between x=0.87m and x=0.94m, the number of turbulent spots increased considerably while between x=0.94m and x=1.07m it is the duration of these spots that has increased.
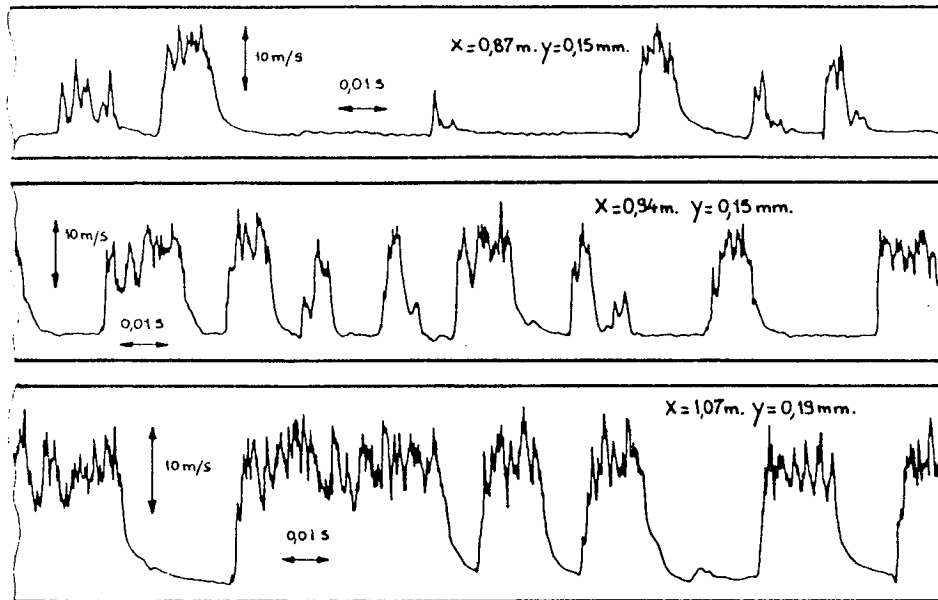
Figure 17 - u' Recordings (x=0.87m; x=0.94m; x=1.07m).

In figures 18 and 19, we show the evolution along y of the signals
recorded at the station x=0.94m. Here again, we compare the simultaneous
recordings of a reference signal near the wall (y_0=0.4mm) and of a signal
at a variable altitude.The relative amplitudes of the two simultaneous
signals are noted on the right side of the recordings. The observation
of these recordings calls for the following remarks:

-Near the wall, the average velocity within the turbulent spots is greater
than the laminar velocity. When y increases, the phenomenon reverses
itself: at y=2.1mm and y=3.5mm, the laminar velocity is greater than the
turbulent velocity. The last two recordings reveal that the beginning of
every spot at y=10mm is indicated by the existence of a positive fluctuation
of very short duration with an amplitude that is nevertheless rather low.

-The appearance of a spot takes place at the same time at all y values. We
have just seen that this remark is valid at y=10mm, or about three times
the $\delta_{0.99}$ thickness of the boundary layer. We were able to check that this
was still true at y=15mm; however, at this altitude the positive fluctuations
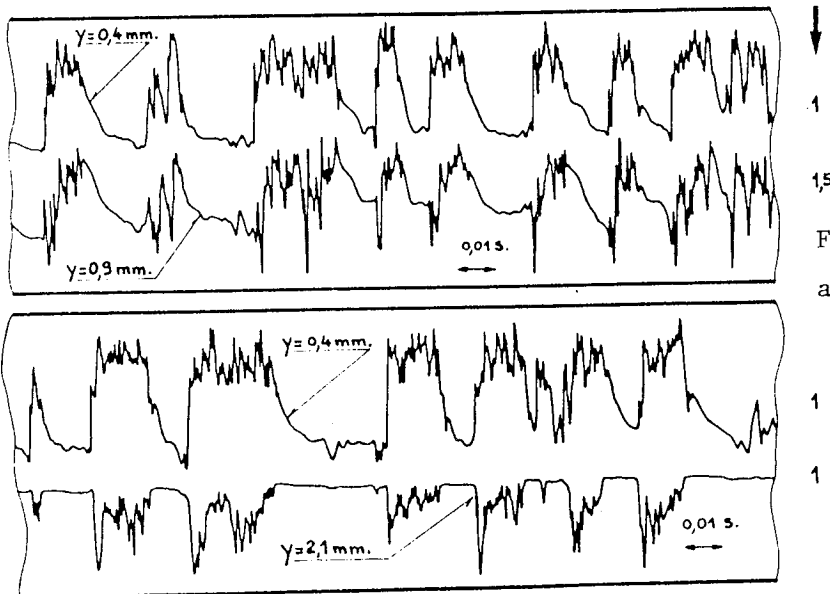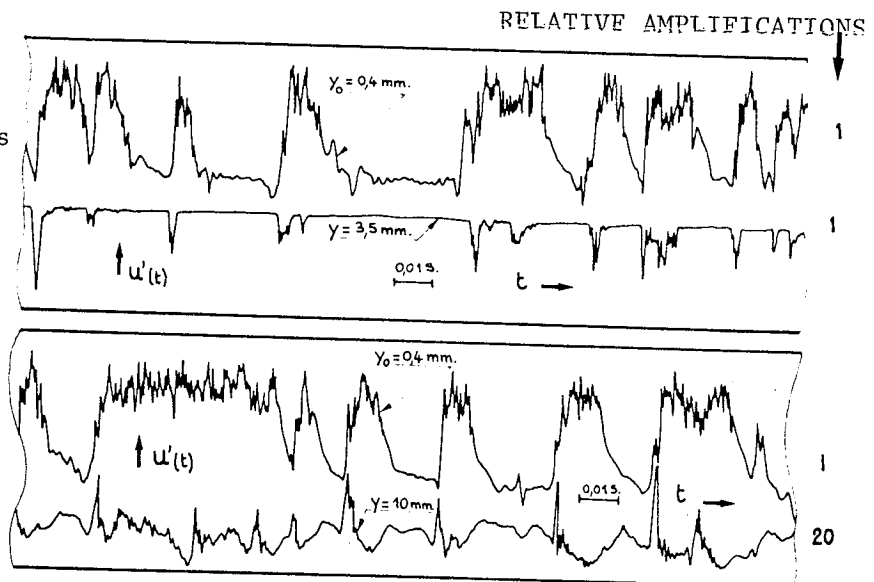
28

RELATIVE AMPLIFICATIONS

Figure 18 - u' Recordings
and Evolution Along y (x=0.94m).

Figure 19 - u' Recordings
and Evolution Along y
(x=0.94m).

RELATIVE AMPLIFICATIONS

29

previously described begin to be difficult to distinguish from the free-
stream turbulence fluctuations. In any case, it appears that if the duration
of a spot decreases with altitude, this decrease takes place starting
from the rear.

-The shape of the spots changes from a nearly symmetrical pulse shape near
the wall to a very unsymmetrical sawtooth when the altitude increases.

-At y=0.9m, we immediately distinguish,before the beginning of the spot,
the negative fluctuation spikes described in the previous paragraph. At
y=2.1mm and at y=3.5mm, they form the leading edge of the turbulent spots.

5.3.2. - Quantitative Study
The detection function selected here is the absolute value of $\delta^2 U/\delta t^2$
smoothed out over four consecutive data acquisition points.

Overall Averages Over a Period of Time: First of all, with respect to the
intermittency factor γ, we have observed (References (5) and (6)) that the
$\gamma(y)$ distributions at the three abscissas considered have a similar shape:
they show a constant level near the wall then decrease slowly to reach
a zero value in the free-stream flow. We generally consider that the
maximum value of γ obtained near the wall is sufficient to characterize
the intermittency at a given abscissa. The maximum values of γ corresponding
to our experiments are respectively: 0.25 at x=0.87m; 0.55 at x=0.94m
and 0.85 at x=1.07m.

The various profiles for average turbulent velocity $U_t/U_e(y)$ and for average
laminar velocity $U_\ell/U_e(y)$ are plotted in Figure 20. We see that, with the
three configurations studied, these profiles cross each other at a y altitude
in the order of a millimeter and that the U_t-U_ℓ difference varies in
accordance with observations made from the recordings in Figures 18 and 19.

Figure 21 shows that, in the case of abscissa x=0.94m, the evolution of the
three contibutions to turbulence $\overline{u'^2}$ and to drag $\overline{-u'v'}$ (turbulent term,
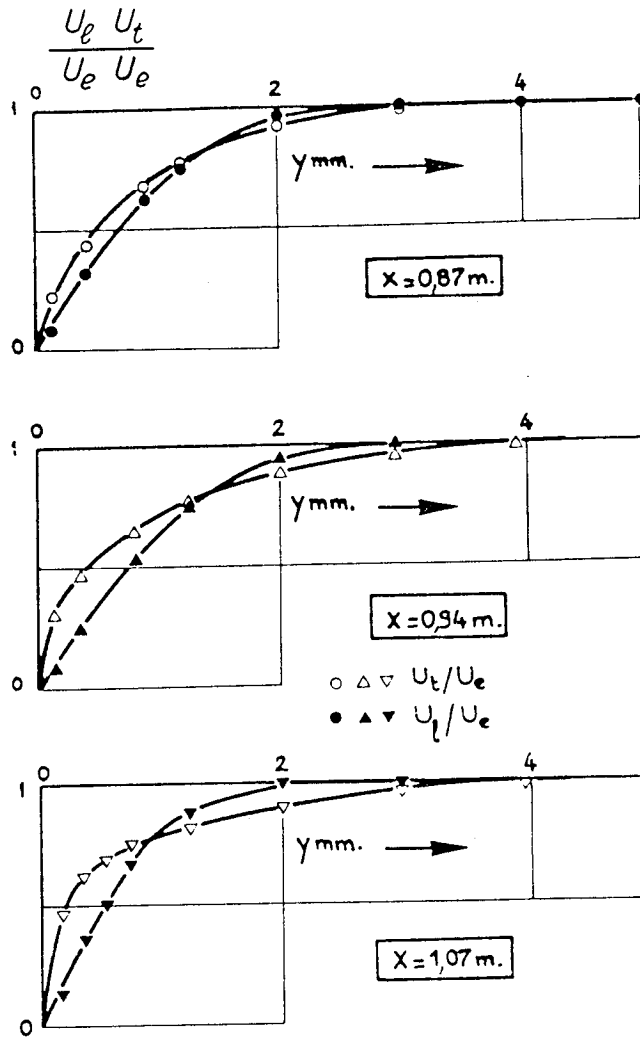
30

Figure 20 - Average Velocity U_t and U_ℓ Profiles.

laminar term and "slot term"). It appears that, near the wall, the "slot" term contributes more than 40 per cent of the overall turbulence energy $\overline{u'^2}$ and provides the explanation for the very high rate of turbulence observed in this area. Moreover, considering the evolution of the U_t-U_ℓ difference, the "slot" term goes to zero then goes to a second maximum located to the position of the second maximum of the coarse profiles. The laminar contribution remains low.
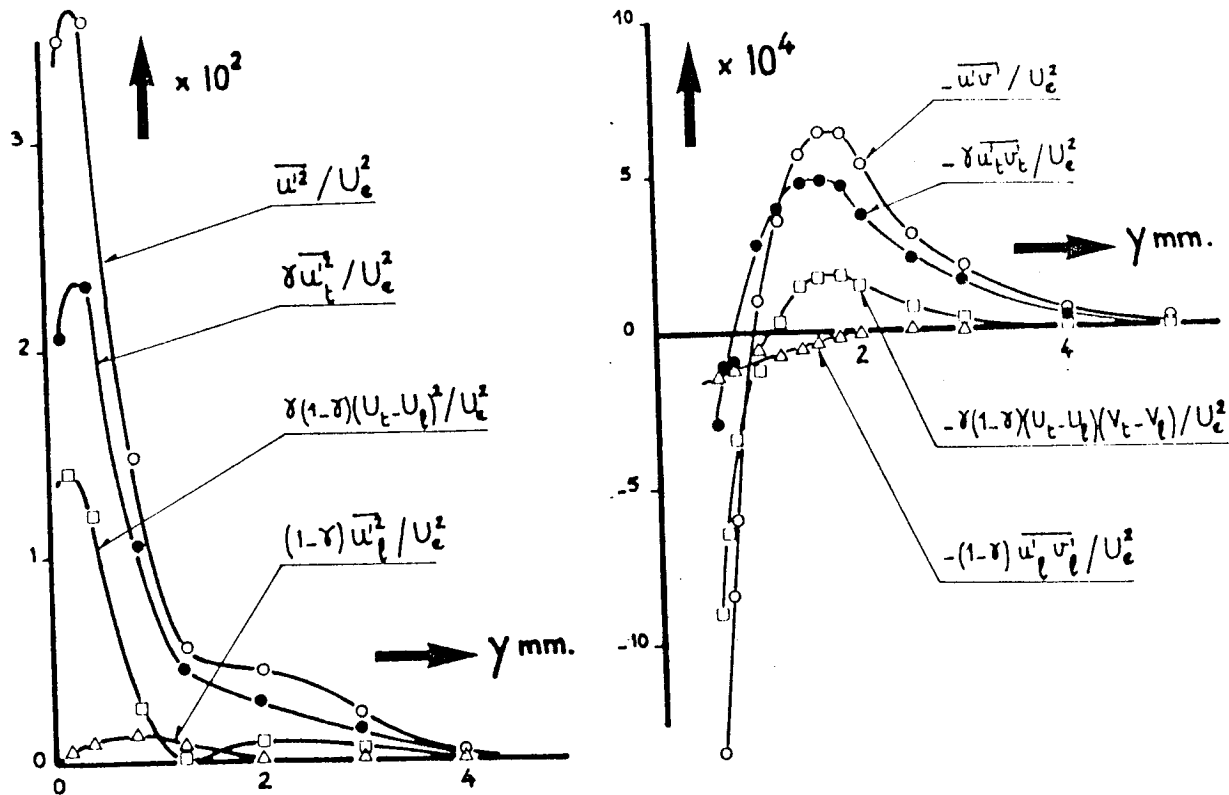
Figure 21 - Breakdown of $\overline{u'^2}$ and $\overline{u'v'}$ (x=0.94m).

The negative portion of the $-\overline{u'v'}$ drag is almost entirely caused by the "slot" term. Inside the positive portion, it is the turbulent term $-\gamma\overline{u'_t v'_t}$ that becomes the most dominant.

Overall Averages at a Given t/T_t: These averages make it possible to establish a "typical portrait" for turbulent spots. We present a certain number of them in Figure 22 with probe points near the wall. The $<U_t>$ (t/T_t) are obtained with spots with a time of passage between the two extreme values given in the figure.
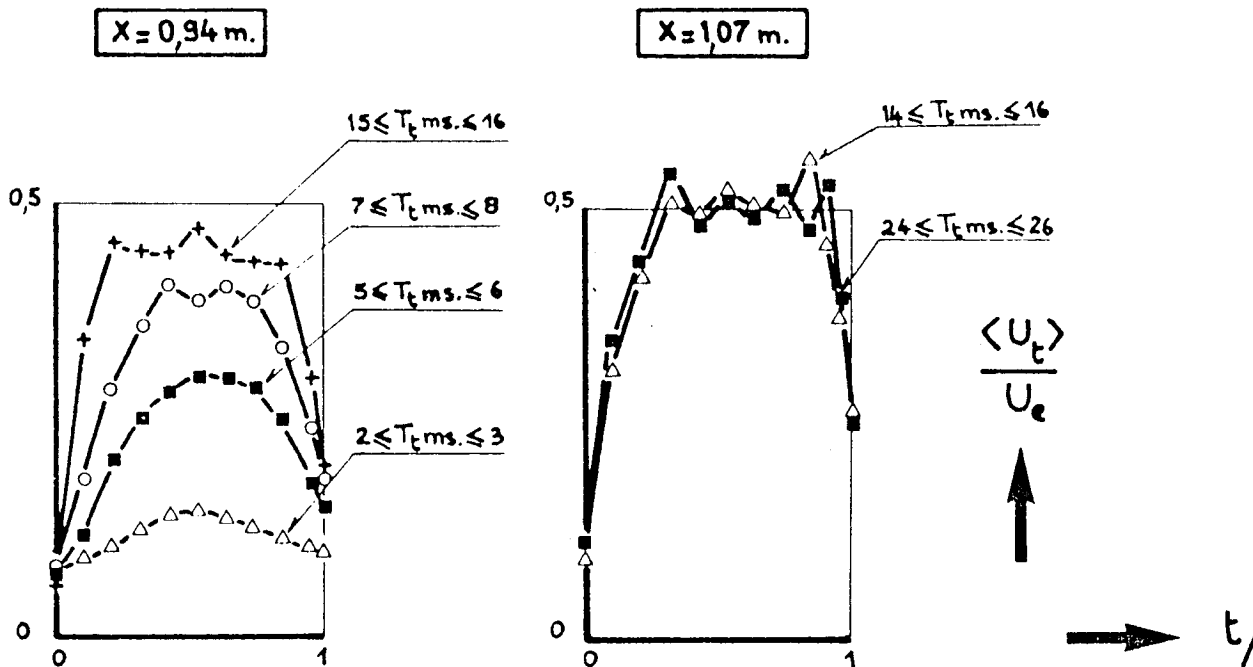
$X = 0,94\,m.$

$15 \leqslant T_t\,ms. \leqslant 16$

$7 \leqslant T_t\,ms. \leqslant 8$

$5 \leqslant T_t\,ms. \leqslant 6$

$2 \leqslant T_t\,ms. \leqslant 3$

$X = 1,07\,m.$

$14 \leqslant T_t\,ms. \leqslant 16$

$24 \leqslant T_t\,ms. \leqslant 26$

$$\frac{\langle U_t \rangle}{U_e}$$

t_1

Figure 22 - Shape of the Spots According to their Duration (x=0.94m; x=1.07m).

We see that in the middle of the transition (x=0.94m), the shape of the
spots changes considerably with their duration: the shape of the curves
is more round for turbulent areas of short duration and becomes more
angular when the time of passage increases. At the same time, we observe
a considerable increase in the maximum value of $\langle U_t \rangle$. On the other hand,
at the end of the transition (x=1.07m), the shape of the spots is
independent of their duration. Examination of recordings in Figure 17
confirms this evolution: at x=0.94m (also at x=0.87m), we encounter spots
with a very different amplitude which is not the case at x=1.07m where
the amplitude does not vary much from one to the other.

Another way to determine the evolution of spots consists of examining how
the maximum value of $\langle U_t \rangle$ varies as a function of the passage duration
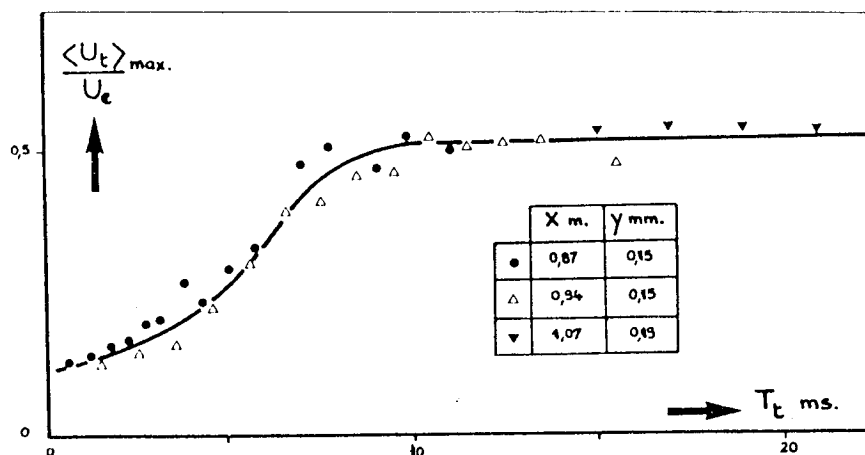
33

	X m.	Y mm.
●	0,87	0,15
△	0,94	0,15
▼	1,07	0,13

Figure 23 - Effect of the Passage Time (Duration) on $<U_t>_{max}$.

(Figure 23). By plotting the points corresponding to the three abscissas
for a nearly constant value of the y/δ ordinate, we obtain a single curve
displaying an increasing segment up to T_t= about 9ms and a level segment
beyond that time.

Study of the Spots with a Duration Greater than 9 Milliseconds: When
considering the spots with a passage duration near the wall greater than
9 milliseconds, we concentrated on determining their turbulent characteristics
by first making overall averages. Figure 24 gives a few examples of the
results obtained in that manner at x=0.94m. The average velocity profile
differs little from a fully established turbulent profile: for this
profile, we found a shape parameter equal to 1.47 (Wygnanski-Sokolov-Friedman
(19) find a 1.50 value for a spot artificially created with an electrical
discharge). The Reynolds shear-stress profile more or less corresponds to
the one that we can encounter within a fully established turbulent boundary
layer; specifically, we no longer observe negative values near the wall.
Finally, the probability density of the u'_t fluctuation is close to the
Gaussian law. Therefore, it is established that we again find within long-
duration turbulent spots a certain number of classical properties of turbulent
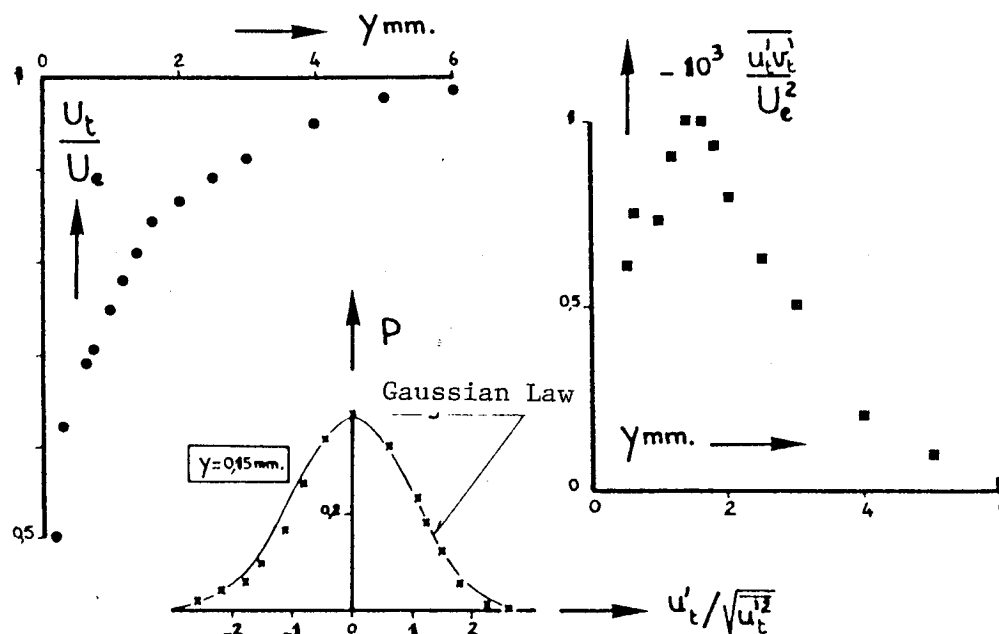boundary layers.

Figure 24 - Study of the Spots with a Duration Greater Than or Equal to 9ms
(Averaged over a Period of Time).

The passage of the spots can be studied in a more precise manner by making
overall averages. We show a few examples of this in Figure 25, still for
station x=0.94m. The various curves were stopped in time so that the leading
edge of the spot appears simultaneously at all altitudes and the passage
duration of this spot decreases along y proportionally to the intermittency
factor. The evolution of the shape of the turbulent spots as a function
of altitude conforms with the observations made from the recordings in
Figures 18 and 19. For altitudes greater than 1mm, we, once again, find
in particular the presence of a very steep leading edge and of a much more
gradual return to the laminar regime. Moreover, we note a similarity in
shape with the results obtained with non-stationary flow (17); this tends
to show that the shape of the spots is independent of free-stream conditions
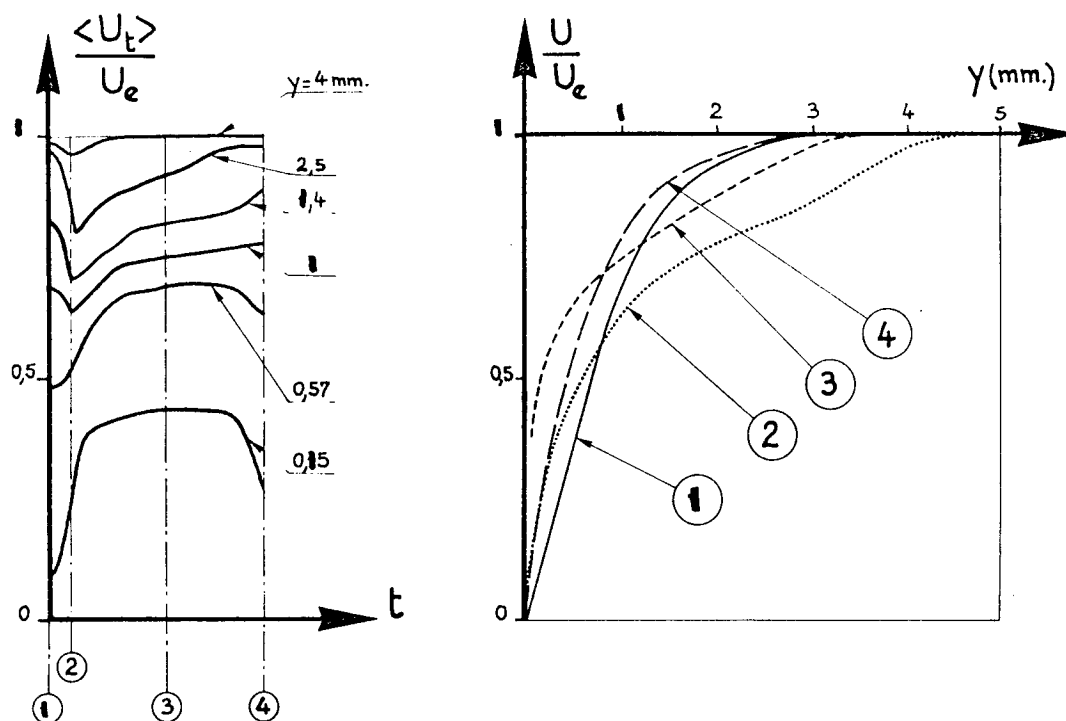and of the mechanism leading to their generation.

Figure 25 - Study of the Spots with a Duration Greater Than or Equal to 9ms
(Overall Averages).

In the right section of the figure, four instantaneous profiles have been plotted. At the very beginning of the spot, the Profile ① is very close to a Blasius profile: its shape parameter is equal to 2.59. Profile ② shows mostly a considerable increase of the boundary layer as well as of the integral thicknesses δ_1 and Θ. Profile ③ shows the largest values of the average speed near the walls but its thickness has already decreased compared with the thickness of the previous profile. Finally, the last profile is entirely above the first (H=1.97).

36

6 - COMPARISON WITH COMPUTATIONS

6.1. - Turbulence Model

As mentioned in the introduction the initial purpose of this experimental study was to check a computation method that we had developed in parallel, a method based on a model with two transport equations for the turbulence kinetic energy $k=\frac{1}{2}(\overline{u'^2}+\overline{v'^2}+\overline{w'^2})$ and its dissipation $\varepsilon= \Sigma\nu\overline{(\frac{\partial u_i'}{\partial x_j})^2}$.

By adopting the modelling proposed at the Imperial College (21)(22), the equations for k and ε are written as:

$$\rho\frac{Dk}{Dt} = -\rho\overline{u'v'}\frac{\partial U}{\partial y} - \rho\varepsilon + 2\mu\left(\frac{\partial k^{1/2}}{\partial y}\right)^2$$
$$+ \frac{\partial}{\partial y}\left(\left(\mu+\frac{C_k}{(2a_1)^2}\mu_t\right)\frac{\partial k}{\partial y}\right)$$

$$\rho\frac{D\varepsilon}{Dt} = -C_{\varepsilon_1}\frac{\varepsilon}{k}\rho\overline{u'v'}\frac{\partial U}{\partial y} - f_2 C_{\varepsilon_2}\frac{\varepsilon^2}{k} + 2\nu\mu_t\frac{\partial^2 U}{\partial y^2}$$
$$+ \frac{\partial}{\partial y}\left(\left(\mu+\frac{C_\varepsilon}{(2a_1)^2}\mu_t\right)\frac{\partial\varepsilon}{\partial y}\right)$$

$$\text{with } -\rho\overline{u'v'}= \mu_t\frac{\partial U}{\partial y} \quad \text{et} \quad \frac{\mu_t}{\rho} = f_\mu(2a_1)^2\frac{k^2}{\varepsilon}$$

$C_{\varepsilon 1}$, $C_{\varepsilon 2}$, C_k, C_ε, a_1 are empirical constants with respective values of 1.57, 2, 0.09, 0.069 and 0.15. Viscosity functions f_2 and f_μ, also empirical, are assumed to depend on the Reynolds turbulence number $R_t=\rho k^2/(\mu\varepsilon)$. We give them the following algebraic formulas:

$$f_\mu = \exp\left(\frac{-2.5}{1+R_t/50}\right)$$
$$f_2 = 1 - 0.3\exp\left(-R_t^2\right)$$

A certain number of applications that we will be able to find in (23) and (24) have shown that this technique leads to coherent results for different problems pertaining to the effects of free-stream turbulence, pressure gradient and heat flux at the wall.

6.2. - Application To Present Experiments

Comparing numerical results with the experiments that we have just described
makes it possible to check in detail the turbulence model used. This
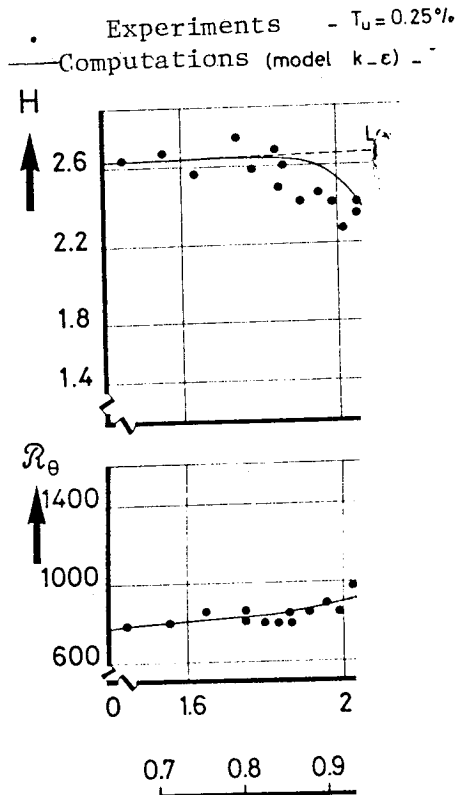comparison is made in Figures 26, 27 and 28.

Figure 26 - Comparison of Experiments and Computations.

Figure 26 shows, with a continuous line, the result of the computation of the
shape parameter and of the Reynolds number R_θ. Agreement with the experimental
points is satisfactory for both locating the triggering of the transition
and for the evolution of the quantities considered up to the turbulent regime.

In Figure 27, the experimental turbulence profiles are compared against
computed profiles. Since the transversal turbulent energy $\overline{w'^2}$ was not
measured, two hypotheses (classical for a turbulent boundary layer) were used
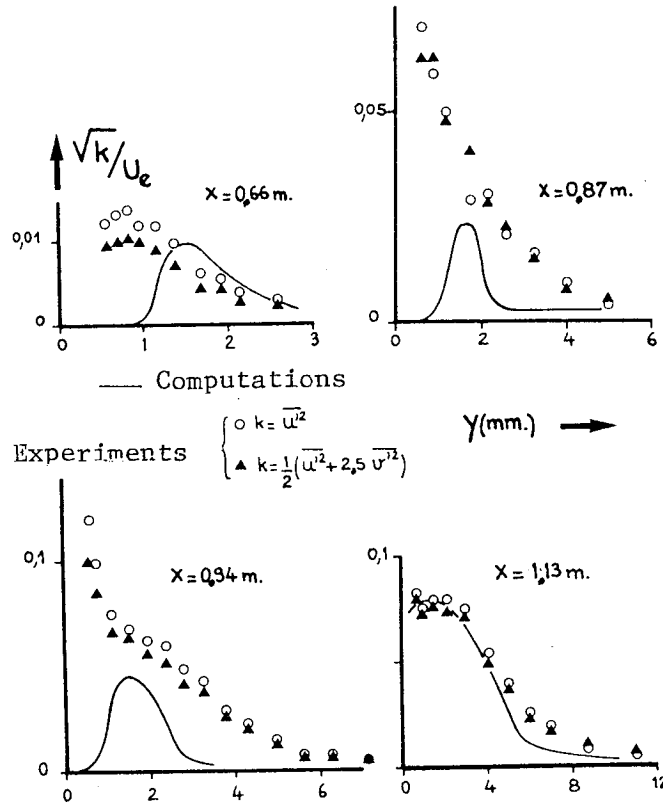to make the comparison: either $k=\overline{u'^2}$ or $\overline{w'^2}=1.5\overline{v'^2}$, that is to say

Figure 27 - Comparison of Experiments and Computations.

$k=\frac{1}{2}(\overline{u'^2}+2.5\overline{v'^2})$. We can see that one or the other of the hypotheses makes it possible to arrive at the same conclusions as to the agreement of experiments with computations. Computations first show a rapid increase in the maximum of kinetic energy; then, starting with x=0.94m, the value of this maximum changes little. Specifically, the very strong turbulence "spike" that experiments have shown near the wall is not found in computations. We have shown that this spike is closely tied to the intermittency phenomenon, a phenomenon that is too complex to be considered in the equations used.

The sign change for the overall drag $-\overline{u'v'}$, also attributable to the intermittency phenomenon, is not reproduced in the computations (Figure 28).

39
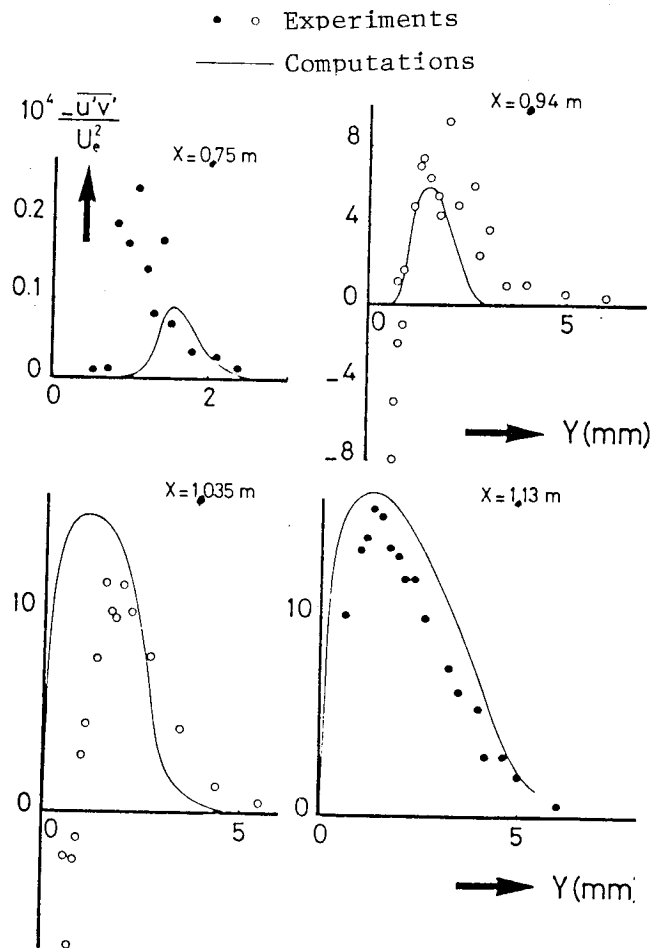
Figure 28 - Comparison of Experiments and Computations.

At the last station where a comparison is made (x=1.13m), the transition is nearly complete and the comparison of experiments vs. computations is entirely correct.

7 - CONCLUSION

Experimental results presented have made it possible to obtain a certain amount of information on the structure of the boundary layer near the transition and during the development of that transition.

40

In a laminar regime, the Tallmien-Schlichting waves, indications of natural instabilities within the boundary layer, obey the laws derived from the theory of laminar instability. The appearance of negative fluctuation spikes of significant amplitude constitute the last stage of the transition process before the first turbulent spots appear. Although hardly frequent, these spikes increase the overall turbulence levels and Reynolds shear stress levels in particular.

The development of the turbulent spots, that is the intermittency, is then the main characteristic characterizing the passing from the laminar to the turbulent state. The overall measurements (U, $\overline{u'^2}$, $\overline{v'^2}$ and $-\overline{u'v'}$) conceal the fundamental mechanisms in that process since the hot wire probes are successively immersed in laminar areas and turbulent spots with very different properties. Conditional Sampling of the instantaneous velocities $U(t)$ and $V(t)$ enabled us to study the two types of flow separately. In particular, we have seen the primordial significant of the "slot" term which explains a certain number of peculiarities in the shape of the coarse $\overline{u'^2}$ and $-\overline{u'v'}$ profiles. Moreover, if we only consider the turbulent spots with sufficient duration, we again find some classical properties found in an established turbulent regime.

A computation method based on the resolution of a system of two transport equations gives the correct position of the triggering of the transition and provides -for the evolution of average values- satisfactory results up to the turbulent regime. Nevertheless, we note on the turbulence and turbulent drag profiles some differences that are clearly attributable to the intermittency phenomenon which modeling cannot take into consideration.

Further experimental studies seem desirable to study the triggering mechanism and the mechanism leading to the generation of the transition under the effect of factors such as free-stream turbulence (level and spectrum) or a pressure gradient. A systematic comparison with the computation results

will then make it possible to test to the maximum extent possible the turbulence model used. It already appears impossible to compute in a precise manner the evolution of turbulent quantities within the boundary layer itself; on the other hand, we can hope to be able to correctly determine the location of the beginning of the transition and of its size within a large range of variations in these factors.

1. Schubauer , G. B., Klebanoff, P. S.: Contribution on the Mechanics of Boundary Layer Transition, Rept. 1289, 1956, NACA.

2. Schubauer, G. B., Skramstad, H. K.: Laminar Boundary Layer Oscillations and Transition on a Flat Plate, Rept. 909, 1948, NACA.

3. Klebanoff, P. S., Tidstrom, K. D., Sargent L. M.: The Three-dimensional Nature of Boundary Layer Instability, J. Fluid Mech., Vol. 12, Part 1, p. 1, 1962.

4. Kovasznay L. S. G., Komoda, H., Vasudeva B. R.: Detailed Flow Field in Transition, Proc. 1962, Heat Transfer Fluid Mech. Inst., Stanford University Press, 1962, 1-26.

5. Arnal, D., Juillen, J. C.: Study of the Intermittency within A Transition Region, La Recherche Aérospatiale No. 1977-3.

6. Arnal, D., Juillen, J. C.: Research in the Transition in Incompressible Flow, N.T. AAAF No. 77-15.

7. Schlichting, H.: Boundary Layer Theory, 6th ed., Mc. Graw-Hill, New York, 1968, pp. 431-522.

8. Jordinson, R.: Numerical Integration of the Orr-Sommerfeld Equation, J. Fluid Mech., Vol. 43, Part 4, (1970).

9. Gaster, M.: On the Effects of Boundary-layer Growth on Flow Stability, J. Fluid Mech., Vol. 66, Part 3, (1974).

10. Fasel, H.: Investigation of the Stability of Boundary Layers by a Finite-difference Model of the Navier-Stokes Equations, J. Fluid Mech., Vol. 78, Part 2, (1976).

11. Ross, J. A., Barnes, F. H., Burns, J. G., Ross, M. A. S.: The Flat Plate Boundary Layer. Part 3. Comparison of Theory with Experiment, J. Fluid Mech., Vol. 43, Part 4, (1970).

12. Burnel, S., Cougat, P.: Study of the Development of the Natural Instabilities within the Laminar Boundary Layer in an Incompressible Flow, C.R. Acad. Sci., Paris, Vol. 274 (April, 1972).

13. Tani, I.: Review of Some Experimental Results on Boundary Layer Transition, Phys. of Fluids, 1967, Supplement 10, p. S11-S16.

14. Knapp, C. F., Roache, P. J., Mueller, T. J.: A Combined Visual and Hot-wire Anemometer Investigation of Boundary Layer Transition, UNDAS-TR-866 CK, August, 1966.

15. Hama, F. R., Long J, D., Hegarty, J. C.: On Transition From Laminar to Turbulent Flow, Journal of Applied Physics, Vol. 18, Number 4, April 1957.

16. Emmons, H. W.: The Laminar-turbulent Transition in Boundary Layer. Part 1., J. Aer. Sc., Vol. 18, 1951, p. 209-298.

17. Cousteix, J., Houdeville, R., Desopper, A.: Transition of a Boundary Layer Subjected to an Oscillation in the Free-Stream Flow, Paper presented to the "Laminar-Turbulent Transition" Symposium. AGARD Fluid Dynamics Panel, Copenhagen, May 2-4, 1977. ONERA TP No. 1977-55.

18. Elder, J. W.: An Experimental Investigation of Turbulent Spots and Breakdown to Turbulence, J. Fluid Mech., Vol. 9, Part 2 (1960).

19. Wygnanski, I., Sokolov, M., Friedman, D.: On a Turbulent Spot in a Laminar Boundary Layer, J. Fluid Mech., Vol. 78, Part 4, (1976).

20. Mithcner, M.: Propagation of Turbulence from an Instantaneous Point Disturbance, J. Aer. Sci., May 1954.

21. Hanjalic, K., Launder, B. E: A Reynolds Stress Model of Turbulence and Its Application to Thin Shear Flows, J. Fluid Mech., Vol. 52, Part 4, (1972).

22. Jones, W. P., Launder, B. E.: The Prediction of Laminarization with a Two-equation Model of Turbulence, Int. J. of Heat and Mass Transfer, Vol. 15, No. 2, (1972).

23. Arnal, D., Juillen, J, C,: Experimental and Theoretical Study of the Boundary Layer Transition, La Recherche Spatiale No. 1977-2, pp. 75-88.

24. Michel, R.: Prediction of the Appearance and Development of the Boundary Layer Transition, ONERA Technical Note No. 1977-6.